8.3 NONMIGRATING TIDES

S. Kato

Radio Atmospheric Science Center, Kyoto University
Gokanosho, UJI, Kyoto 611, Japan

Recently we have seen an interesting advancement in the study of nonmigrating tides. There have been two distinct approaches in works on this subject. One is based on mechanistic models as considering nonuniform global distribution of water vapor or heating only on land, solving a set of linear equations. It is found that insolation absorption of the nonuniformly distributed water vapor produces only weak nonmigrating tides in the lower thermosphere; the planetary boundary layer heating on land can explain the enhanced tides on land and those with short vertical wavelengths in the stratosphere. The other approach is novel and uses simulation on the general circulation model (GCM). This realistic model can reproduce tides globally and in many details. The enhancement of two nonmigrating modes as eastward traveling modes with a wave number 3 and westward traveling modes with a wave number 5 is in surprisingly good agreement with observation at sea level, at 700 mb and even at 300 mb.

Table 1. Parameters in various works.

CASE	Heat Source	Model	Resolution *etc.*
1	Water vapor insolation absorption	EGW dissipation No winds	$s = -2, -1, 0, 1, 2, 3$ for $n = 1$ plus $s = 1$ for $n = 2$ $\Delta z = 0.5 - 1.0$km $80 < z < 100$km
2,3	GCM(IMR)	GCM(IMR)	$\Delta\theta = 4°$ $\Delta\phi = 5°$ Δz : 12 *levels* $\sim$ 5km $P_0 > 1$mb
4	P.B.L.heating	Classical tidal theory only with Newtonian cooling	$\|s\| \leq 20, \|n\| \leq 20$ $\Delta z = 40$m MST region

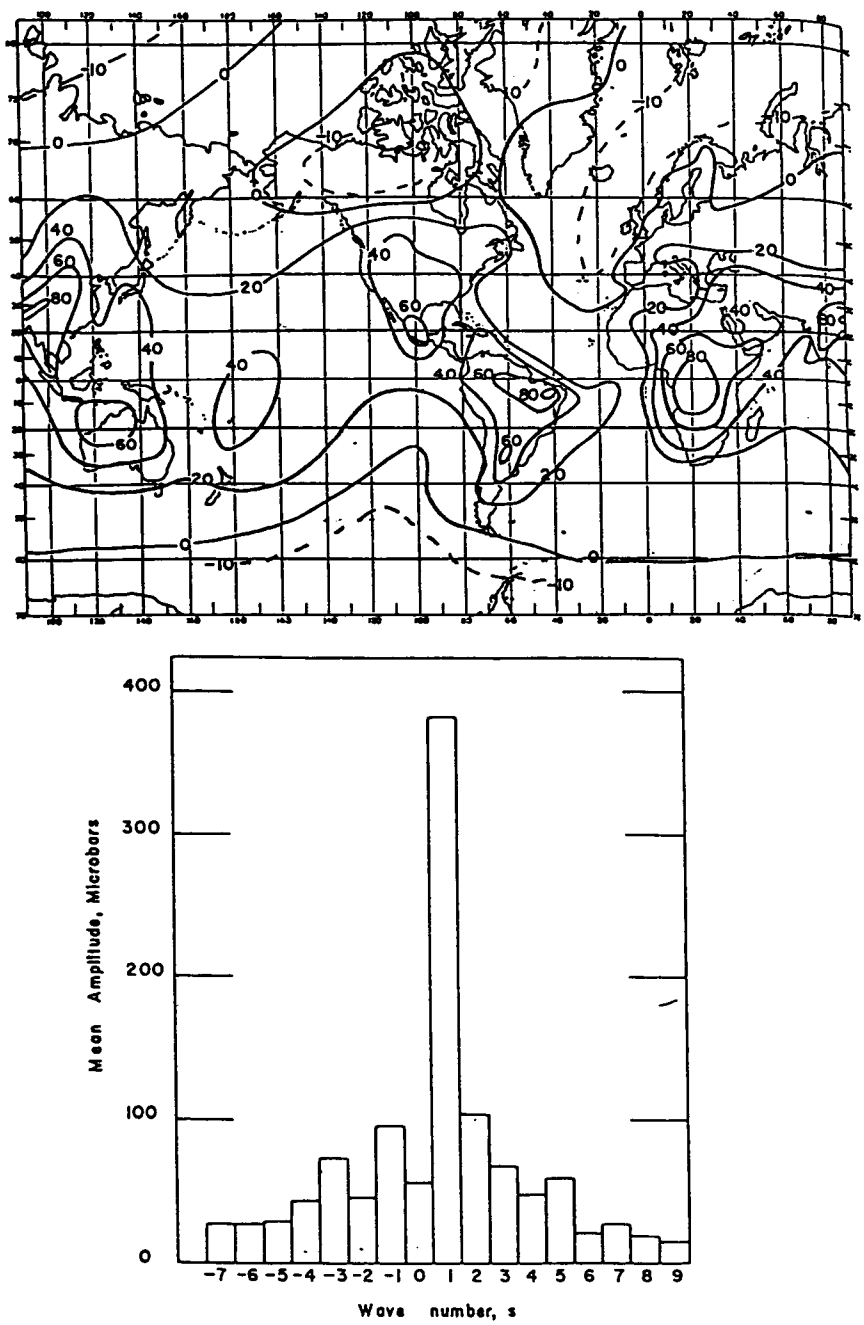

Figure 1. Diurnal tides observed at sea level global distribution (top), wave number spectrum averaged along latitudes (bottom) [Haurwitz, 1965].

$p = 1$ from b, $\chi = 2.3$

$\chi = \ln\left(\frac{p_0}{p}\right)$

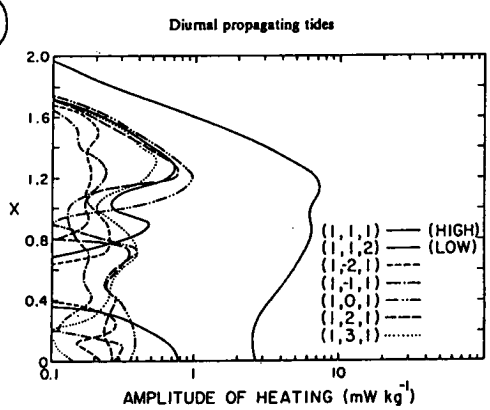

Figure 2. Vertical profiles of diurnal heating in spring equinox for various modes; x = $\ln(P_0/P)$ where P is the atmospheric pressure and P_0 is P at sea level [Forbes and Groves, 1986].

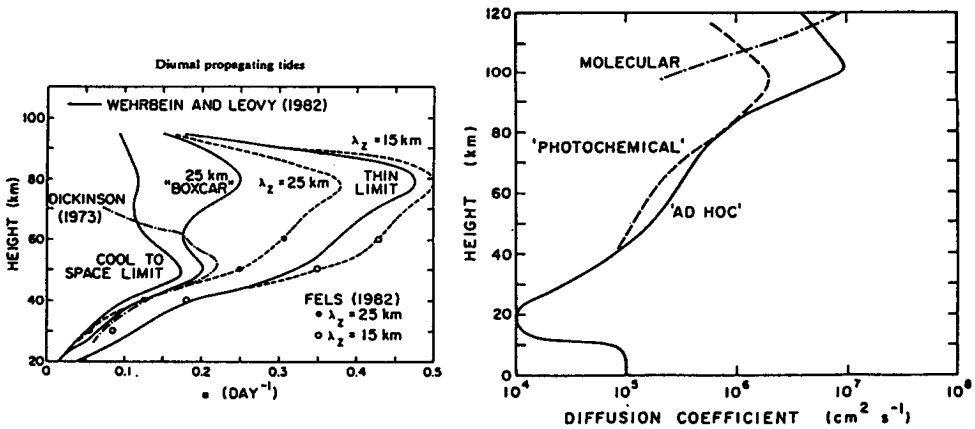

Figure 3. Dissipation rate: Newtonian cooling coefficients. The dashed curves represent profiles used for calculation depending on vertical wavelength λ_z (left), diffusion coefficient (right) [Forbes and Groves, 1986].

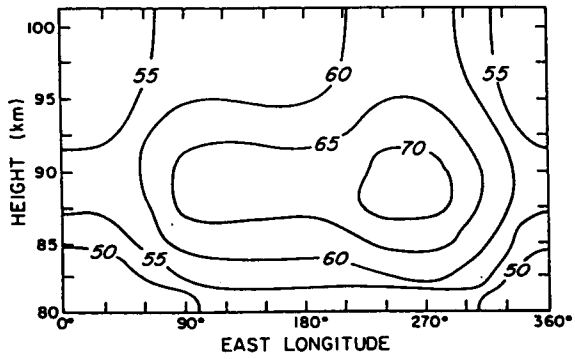

Height–longitude contours of diurnal northward wind amplitude ($m\,s^{-1}$) at 18° latitude for spring equinox assuming *ad hoc* eddy diffusion model.

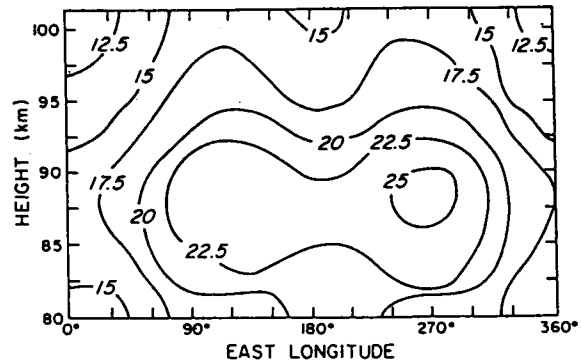

Height–longitude contours of diurnal eastward wind amplitude at 12° latitude for spring equinox assuming *ad hoc* eddy diffusion model.

Figure 4. Calculated winds [Forbes and Groves, 1986].

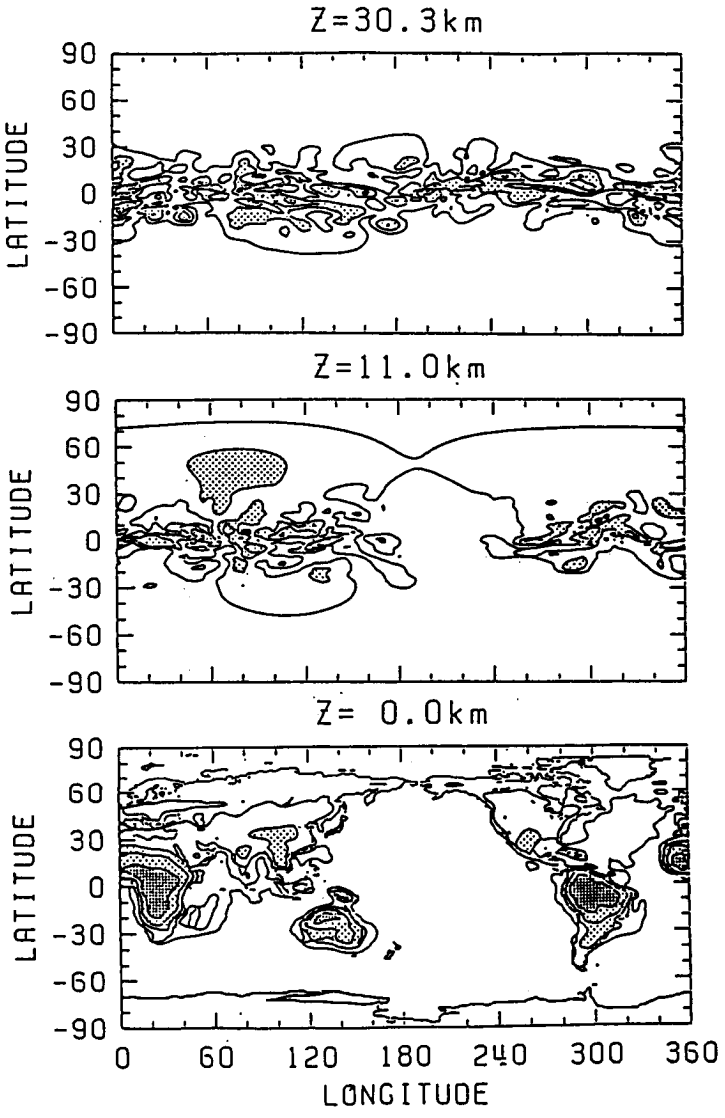

Figure 5. Calculated diurnal pressure tides at equinox [Tsuda and Kato, 1988].

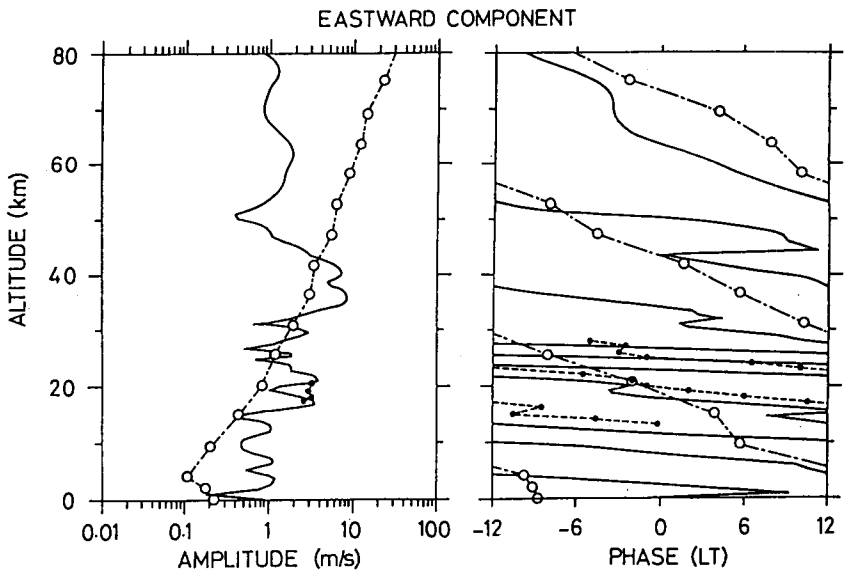

Figure 6. Same as Figure 5 except for vertical profiles of tidal winds.

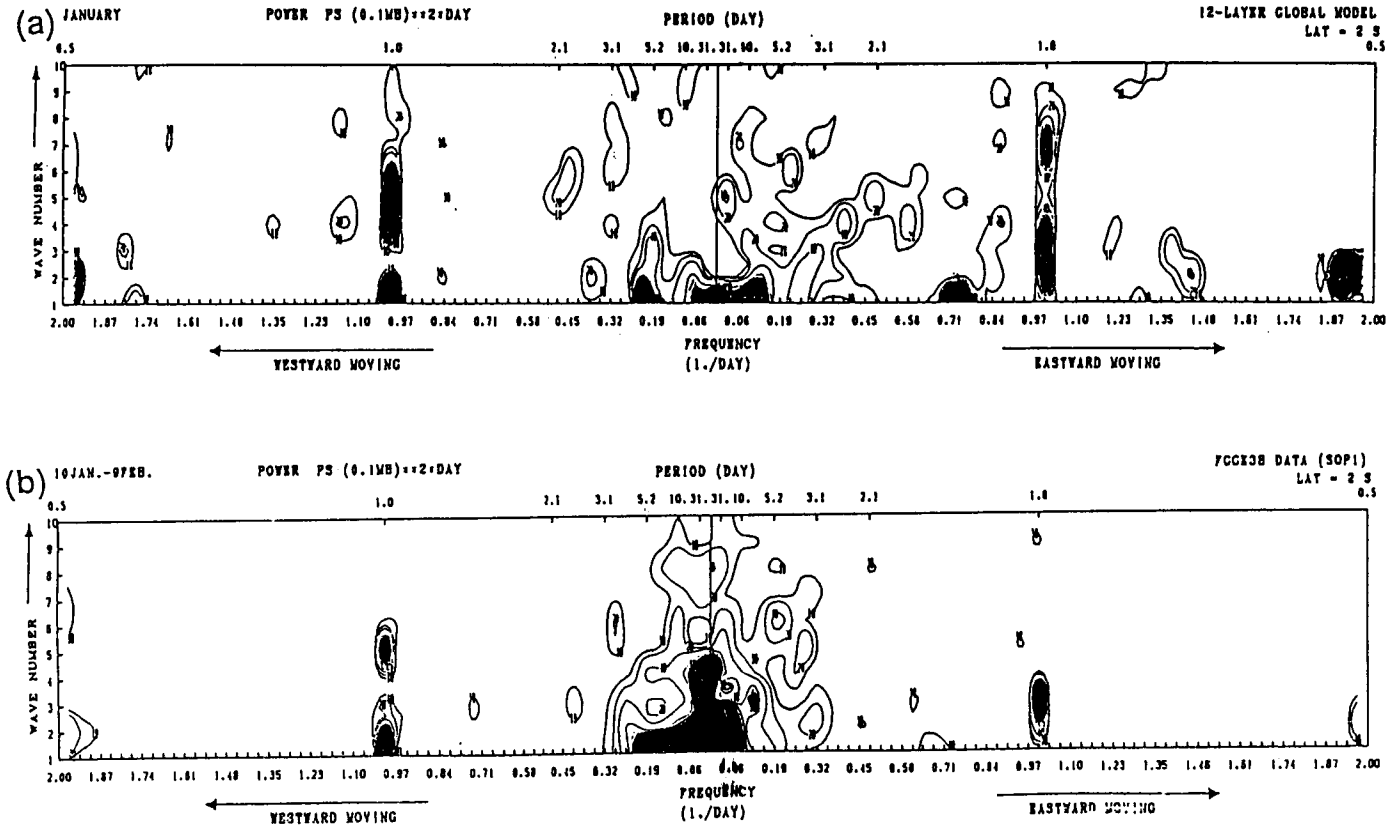

Figure 7. The power spectra of the sea level pressure field in the space-time domain at 2°S from (a) the GCM simulation and (b) FGGE (First GARP Global Experiment) data analysis [Yagai, 1988].

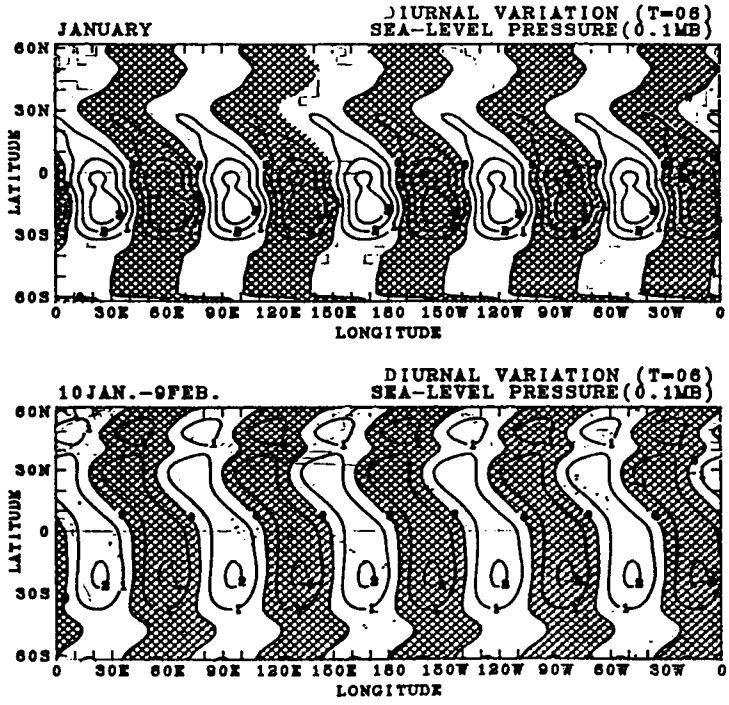

Figure 8. The horizontal map of sea level pressure field of the diurnal mode (s = 5) at 0600 GMT from (a) the GCM simulation and (b) FGG data analysis. The contour interval is 0.1 mb, and negative values are shaded.

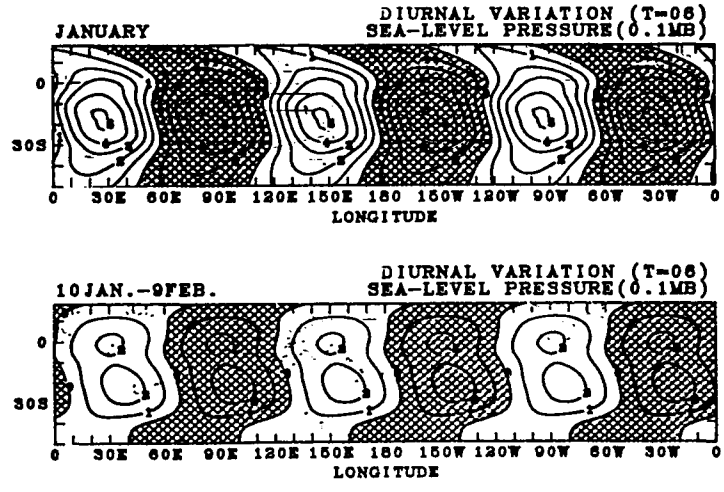

Figure 9. Same as Figure 8 except for s = –3.

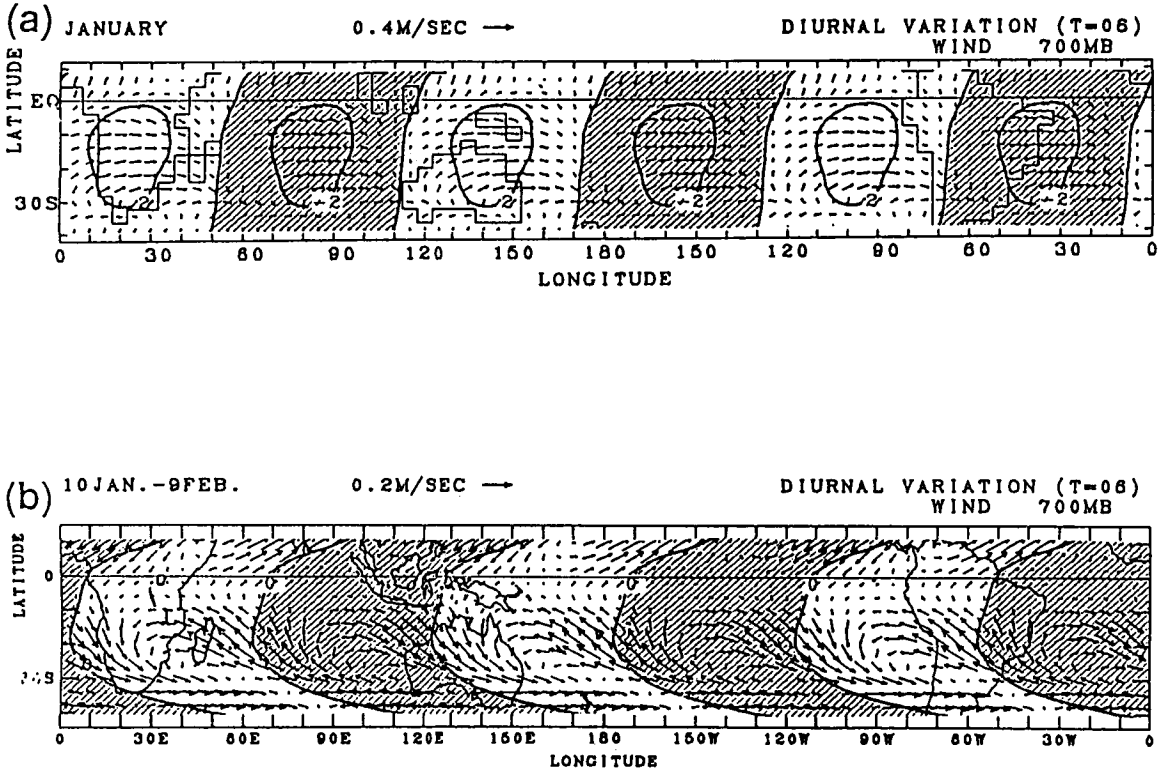

Figure 10. Same as Figure 9 except at 700 mb.

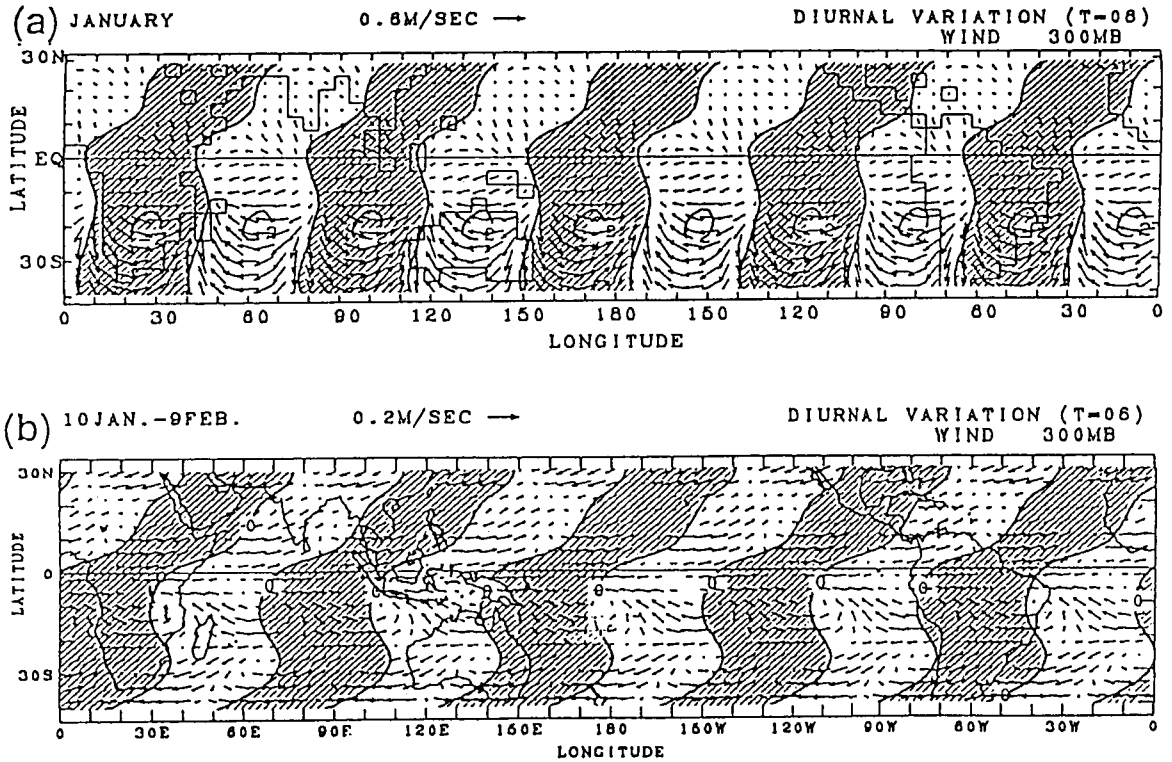

Figure 11.Same as Figure 8 except at 300 mb.